ELSEVIER

Contents lists available at ScienceDirect

### Construction and Building Materials

journal homepage: www.elsevier.com/locate/conbuildmat



## Insights into mechanothermal activation of kaolinite: A novel multistep process for cement precursors

Adrian Alvarez-Coscojuela , Jofre Mañosa , Josep Marco-Gibert , Javier C. Córdoba, Josep Maria Chimenos

Departament de Ciència de Materials i Química Física, Universitat de Barcelona, C/ Martí i Franquès 1, Barcelona 08028, Spain

#### ARTICLE INFO

# Keywords: Mechanothermal activation Mechanochemical activation Thermal activation Pozzolanic activity Supplementary cementitious materials Kaolin Metakaolin

#### ABSTRACT

This study introduces a novel method for activating kaolinitic clays through mechanothermal activation (MTA), combining mechanical activation (MA) and thermal treatment to enhance kaolin's pozzolanic reactivity at lower temperatures than traditional thermal activation (TA). MA effectively lowers kaolin's dehydroxylation temperature, releasing significant hydroxyl groups at just 300 °C. Thermogravimetric analysis data confirms that implementing MTA unlocks the kaolinite dehydroxylation at 300 °C and 400 °C to a great extent and allows almost complete dehydroxylation at 500 °C. X-ray diffraction, surface area analysis, and particle size measurements revealed kaolin's structural changes under MA, TA, and MTA treatments. The pozzolanic values achieved through MTA are significantly higher than those obtained with MA and TA at 300 °C, 400 °C, and 500 °C, as evidenced by reactivity tests. By enabling kaolinite activation at lower temperatures, MTA fosters a promising approach for developing sustainable building materials with a reduced carbon footprint.

#### 1. Introduction

Conventional clinker production is among the largest CO<sub>2</sub> emission sources, causing approximately 5–7 % of the global carbon footprint [1]. Ordinary Portland cement (OPC) obtention entails calcinating raw materials at 1450 °C, involving significant energy consumption and CO<sub>2</sub> release [2]. To address these environmental consequences, the investigation efforts aim to decrease CO2 emissions by developing novel cement formulations with reduced environmental impact [3]. Clay minerals have emerged as a sustainable candidate to totally or partially replace OPC to address this challenge. Kaolinite (Kaol, Al<sub>2</sub>[Si<sub>2</sub>O<sub>5</sub>](OH)<sub>4</sub>) is one of the most abundant clay minerals globally, widely utilised to meet the vast demand of the construction industry [4]. The crystalline structure comprises a sequence of stacked layers formed by silicon tetrahedral and aluminum octahedral sheets arranged in a laminar configuration [5]. Accordingly, this well-ordered conformation limits the Kaol reactivity performances, restricting the potential capability of forming cement-hydrated phases. Consequently, the kaolinitic structure requires amorphising procedures to improve its ability to react, enabling its appropriate use as supplementary cementitious material (SCM) and alternative cementitious material (ACM) precursor [6–8].

As a result, there has been growing interest in the structural

In this sense, the mechanochemical activation (MA) of Kaol has recently emerged as a sustainable replacement for TA [16,17]. MA involves the disruption of kaolinite's chemical bonds through grinding Kaol in a highly energetic milling process [18]. This crystalline structure breakage results in an amorphous material with promising pozzolanic properties [19,20]. The amorphisation degree is affected by the mill type, milling time, rotation speed (for planetary mills), and ball-to-sample ratio, among other parameters [21,22]. MA represents a notable advancement in environmental sustainability, as it replaces

E-mail address: jofremanosa@ub.edu (J. Mañosa).

crystalline distortions of Kaol through thermal activation [9]. Heating Kaol in the range between 400 °C - 650 °C causes hydroxyl loss (dehydroxylation) [10]. This OH removal induces several modifications to Kaols' structure, which acquires a great amorphisation degree, embracing the highest pozzolanic activity values over all SMCs [11,12]. The resulting amorphised material is extensively known in this field of research as metakaolin [13]. In practice, submitting Kaol at 800 °C typically maximises the resultant material reactivity in comparison to higher or lower calcination temperatures [14]. Even though clinkerization process requires much higher temperatures, thermal activation (TA) at 800 °C still entails significant energetic demands at the industry scale, as the kilns used require fuel sources such as coal, and petroleum coke among others [15].

<sup>\*</sup> Corresponding author.

thermal energy with electric energy in the obtention of amorphous aluminosilicate materials [23,24]. This implies a significant reduction in greenhouse gas (GHG) emissions. Despite this, the main drawback of MA compared to TA is the limited reactivity performance with relatively lower pozzolanic values, according to the literature [21,23,25].

In contrast to TA, the amorphisation of the kaolinitic structure induced by MA does not involve hydroxyl loss. Instead, the mechanical treatment detaches hydroxyl groups from the structure, enabling their gradual release at lower temperatures [18]. Leveraging this phenomenon, this research focuses on implementing a low-temperature thermal treatment after MA on Kaol structures. This strategy aims to obtain a highly reactive material at calcination temperatures lower than 800  $^{\circ}\mathrm{C}$  through a mechanothermal activation (MTA) multistep method. Combining MA with TA is particularly appealing due to its potential to significantly reduce fuel consumption in industrial applications, enabling lower-energy processes on a large scale, and thereby reducing the carbon footprint of clay activation.

In this research, MTA was evaluated using various characterisation techniques to analyse the evolution of structural amorphisation and the behaviour of hydroxyl groups under thermal treatments applied to kaolinite after different MAs. Furthermore, reactivity tests were conducted to assess the pozzolanic activity of Kaol subjected to mechanical, thermal, and mechanothermal treatments.

#### 2. Materials and methods

#### 2.1. Materials

The kaolin (K) used in this study without any further purification was provided by the Spanish company Minerals i Derivats, S.A. The chemical composition was analysed using X-ray fluorescence (refer to Table 1) with a Panalytical Philips PW 2400 sequential X-ray spectrophotometer, accompanied by UniQuant® V5.0 software.

#### 2.2. Methods

Mechanical activation (MA): Physicochemical modifications in kaolin were induced via a mechanochemical grinding process conducted with a planetary ball mill PM 100 from RETSCH company. This treatment used Zirconia jars of 500 mL of volume and 10 mm-diameter zirconia balls as accessories. The jars were filled to approximately 20 % of their volume, maintaining a ball-to-sample mass ratio of 20:1. Rotation speed and milling duration were defined in Table 2 to examine their effects on the material. These parameters were adjusted based on recent experimental data [26,27].

Thermal activation (TA): TA has been assessed by heating the samples from room temperature using a Hobersal JB20 muffle furnace with a maximum operating temperature of  $1100\,^{\circ}$ C. The samples were heated for two hours (with different heating rates) to reach the target calcination temperature. At each temperature setpoint, the residence time was established at one hour to ensure effective calcination.

*Mechanothermal activation (MTA):* MTA was performed by initially applying MA, followed by TA. The milling process and calcination temperature were varied to study the effect of these parameters on the activated kaolin. The methodology of milling and calcination was the same as that described for MA and TA.

The parameters for the three distinct activation methodologies parameters are summarised in Table 2. A brief explanation of the sample nomenclature is provided as follows: The mechanically activated

samples are described as KM-rpm-t, where rpm refers to the rotation speed of the grinding process in revolutions per minute, and t is associated with the grinding time in minutes. The thermally treated samples are labelled as KT-T, where T refers to the temperature used for the calcination procedure. In particular. Notably, KT-800 is attributed to metakaolin described in the literature [28–30]. The mechanothermally activated samples are described as K(A or B)-T, where A refers to KM-350–120 and B to KM-300–60, with T denoting the posterior calcination temperature of the MTA. Thus, MTA is emphasised as a multistep process of activation.

#### 2.3. Characterisation techniques

Thermogravimetric analysis (TGA) was conducted to investigate the dehydroxylation behaviour of mechanically treated kaolin, thereby elucidating the mechanothermal phenomenon. Moreover, the TGA of thermally and mechanothermally treated samples was also implemented to compare the effectiveness of the mechanothermal procedure by analysing the differences in dehydroxylation rates. This was carried out using a TGA 550 (TA Instruments) in the temperature range of 30-800 °C, with a heating rate of 10 °C·min<sup>-1</sup> and a nitrogen flux rate of 50 mL·min<sup>-1</sup>. The dehydroxylation degree is determined by first quantifying the mass loss corresponding to non-dehydroxylated hydroxyl groups (OHs) in the TGA analysis of the mechanothermally treated samples  $(m_{MTA})$  [31]. This value is then subtracted from the total mass of OHs during the dehydroxylation of untreated K  $(m_K)$ , thereby providing the amount of OHs dehydroxylated during the mechanothermal treatment alone. Then, dividing this result by the total mass of OHs subject to dehydroxylation in untreated K yields the dehydroxylation degree, as described in Eq. 1.

Dehydroxylation degree = 
$$\frac{m_K - m_{MTA}}{m_K} \cdot 100$$
 (1)

The crystalline composition was determined through X-ray diffraction (XRD) utilising PANalytical X'Pert PRO MPD alpha1 powder diffractometer, operating in Bragg-Brentano  $\theta/2\theta$  geometry with a radius of 240 mm. The system utilised Ni-filtered Cu  $K_\alpha$  radiation with a wavelength of  $\lambda=1.5418$  Å, operating at a power of 45 kV and 40 mA. A mask was used to define a beam length of 12 mm in the axial direction over the sample. Both the incident and diffracted beams were passed through 0.04 rad Soller slits, with a fixed divergence slit of 0.25°. Data were collected using a PIXcel detector with an active length of  $3.347^\circ$ . The scan range was set from  $4^\circ$  to  $100^\circ$  20, with a step size of  $0.026^\circ$  and a measurement time of 100 s per step. The main crystalline phases of the raw kaolin were examined using the X'Pert HighScore software.

Dynamic light scattering (DLS) was utilised to assess the particle size distribution. Measurements were conducted using a laser diffraction particle-sizing analyser (LS 13 320, Beckman Coulter) with the activated kaolins dispersed in ethanol.

The Brunauer–Emmett–Teller (BET) method was conducted to evaluate the specific surface area, providing insights into reactivity behaviours in relation to the structural changes experimented on the material's surface area. This technique was performed through a Micromeritics Tristar 3000 device.

#### 2.4. Reactivity assessment

 $R^3$  test: The  $R^3$  test was conducted in accordance with ASTM C1897 – 20 [32,33]. Different activated samples were mixed with Ca(OH)<sub>2</sub> (at a

Table 1
XRF analysis of the kaolin material.

Compounds	$SiO_2$	$Al_2O_3$	K <sub>2</sub> O	$Fe_2O_3$	CaO	$TiO_2$	Na <sub>2</sub> O	MgO	$P_2O_5$	MnO	LOI*
wt%	49.85	36.31	0.69	00.47	0.16	0.15	0.13	0.11	0.08	0.00	12.03

<sup>\*</sup> LOI: Loss on ignition at 1000 °C.

Table 2
Summary of samples subjected to MA, TA, and MTA treatments.

Sample	Activation methodology	Rotation speed (rpm)	Grinding time (min)	Calcination temperature (°C)	Calcination time (min)
К	-	-	-	-	-
KM - 350 - 120	Mechanical (A)	350	120	-	-
KM - 300 - 60	Mechanical (B)	300	60	-	-
KT-T	Thermal	-	-	300, 400, 500, 600, and 800	60
K(A)-T	Mechanothermal	350	120	300, 400, 500, 600, and 800	60
K(B)-T	Mechanothermal	300	60	300, 400, 500, 600, and 800	60

1:3 ratio) and  $CaCO_3$  (at a 2:1 ratio) and combined with a  $K_2SO_4$  and KOH solution to form a paste, with a solution-to-solid ratio of 1.2. The solution was prepared by dissolving 4 g of  $K_2SO_4$  and 20 g of KOH in 1 L of distilled water. The paste was prepared by mixing the solid components and the solution for 2 min at 880 rpm using a high-shear mixer. Subsequently, 15 g of the paste was transferred into a plastic ampoule. The heat of the reaction was monitored over 7 days using a TAM Air isothermal calorimeter (TA Instruments), maintained at 40 °C. A plastic ampoule containing 9.4 g of water was used as a reference to minimise the contribution of external temperature fluctuations. Additionally, the initial calorimetry data were recorded after 75 min to allow the calorimeter to stabilise at 40 °C and avoid any unstable signals.

In addition, TGA and XRD analyses of the resultant pastes from the  ${\bf R}^3$  test are conducted to track the portlandite consumption as well as the new phases formed during the pozzolanic test, serving as an independent method for assessing reactivity beyond the tests used. Both techniques are performed under the same conditions described above. To ensure the reaction stoppage, the  ${\bf R}^3$  pastes were dried with isopropanol as described by K. Weise [34]. The crystalline phases of the  ${\bf R}^3$  pastes were semiquantified through Rietveld refinement of the diffractograms. The amorphous content was estimated by introducing a single peak to fit the amorphous halo, and the content of crystalline phases was renormalised considering the amorphous content estimation.

Modified Chapelle test: The pozzolanic activity of the activated clay was also assessed through the modified Chapelle test, aimed at quantifying the reactivity of aluminosilicate materials with portlandite [35, 36]. A total of 1 g of SCM and 2 g of powdered CaO were added to 250 mL of distilled water, and the mixture was vigorously stirred for 16 h at 90 °C, with temperature control maintained by refrigerant equipment. A blank test without the pozzolanic material was performed using identical conditions. After cooling the reaction system for 1 h, 250 mL of a 0.7 M sucrose solution was added and mixed for 15 min. Approximately 150 mL of the resulting mixture was then filtered, and 25 mL of the filtrate were titrated with 0.1 M HCl, using 2 drops of phenolphthalein as indicator. The pozzolanic activity (PA), expressed as the amount of portlandite (CH), Ca(OH)<sub>2</sub> fixed by the SCM, was expressed using the following formula:

$$PA = 2 \cdot \frac{\nu_1 - \nu_2}{\nu_1} \cdot \frac{74}{56} \cdot 1000 \tag{2}$$

where PA represents the amount of fixed  $\text{Ca}(\text{OH})_2$  in milligrams per gram of SCM (mg·g<sup>-1</sup>). In this formula,  $v_1$  refers to the volume of 0.1 M HCl required to titrate 25 mL of the control solution, and  $v_2$  is the volume needed to titrate 25 mL of the solution where the pozzolanic reaction has occurred.

Reagents: The pozzolanic activity tests required CaO and  $K_2SO_4$ , both purchased from Thermo Scientific. Fisher Scientific® supplied KOH and Ca(OH)<sub>2</sub>. Additionally, 0.1 N HCl, provided by Labkem, was used for titrations, along with D(+)–Sucrose AGR. All reagents were of analytical grade.

#### 2.5. Energetic assessment

A lab-scale evaluation of electrical consumption associated with the three clay activation methods implemented in this research was

conducted to evaluate the energy impact of MTA. The results are preliminary, as the scalability to industrial levels remains a challenge due to equipment constraints and limited availability of data on MA process in an industrial context. This assessment is not intended to serve as an energy audit, as no efforts were made to optimise the activation processes. The energy consumption used for all the activation procedures is expressed in Wh, based on monitoring data from a power meter connected to each device (furnace or ball mill). In this context, the ball mill, with a 25 g capacity per activation batch, has the lowest throughput. This configuration allows for maintaining a constant ball-to-powder ratio (BPR), optimised in previous trials. The 25 g of mechanically treated raw material are subsequently transferred to the furnace for thermal treatment during MTA. To evaluate MTA efficiency in terms of reactivity yield versus energy use, energy consumption per unit weight is normalised by the cumulative heat release obtained from the R<sup>3</sup> test at 7 days.

#### 3. Results and discussion

#### 3.1. Mechanothermal activation (MTA) concept

The structure modifications caused by the grinding process during the mechanochemical activations do not involve the OHs release. Notwithstanding, the remaining OH become less attached to the Kaol structure because of this distortion process, thus predisposing them to interact more easily [18]. A reduction in the dehydroxylation temperature is observed as a result of the amorphisation induced by MA, as mechanically activated samples exhibit a shift in the thermogravimetric curves (solid line) compared to untreated kaolin (Fig. 1). Accordingly, this phenomenon is exploited in this study to obtain the total dehydroxylation at lower temperatures, requiring less energy or fuel sources during calcination processes. For this purpose, the two mechanically activated K samples (KM-350–120 and KM-300–60) are then heated to 300, 400, 500, and 600 °C, constituting the multistep MTA process, as

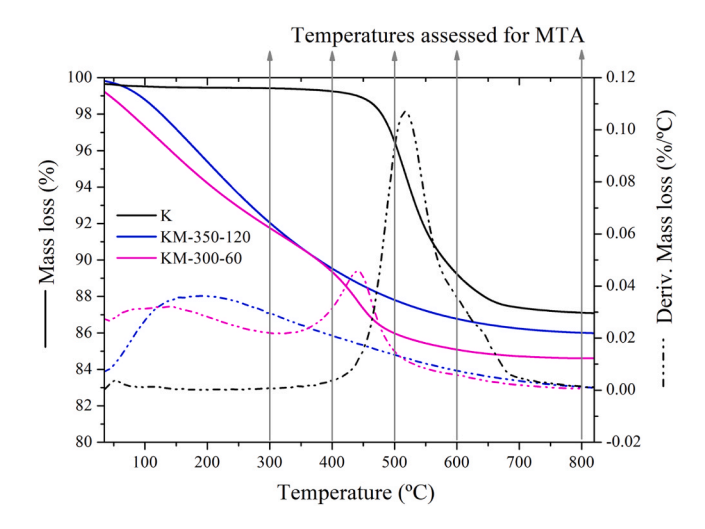


**Fig. 1.** Mechano-thermal activation concept explained through TGA and DTG of mechanically activated K and raw K.

depicted in Fig. 1 with the vertical grey arrows. Additionally, mechanothermally activated K at 800  $^{\circ}$ C is analysed for comparison with MK.

Focusing on the TGA curves, both mechanically activated samples present a mass loss attributed to the dehydroxylation in the region between 100 and 500–600 °C. In contrast, the thermal treatment applied to untreated K shows the OHs decomposition occurring around 520 °C lasting until ~700 °C, as highlighted by the derivative thermogravimetry (DTG). This corroborates the OHs' easy release after submitting K to mechanical grinding. Nevertheless, the mechanical treatment parameters play a crucial role, as their intensity marks the dehydroxylation reduction degree according to the structural disruption accomplished through the MA. Specifically, increasing the MA intensity, as in the KM-350–120 sample, leads to a very low-temperature peak dehydroxylation (see DTG curve). On the other hand, with lower grinding intensity, as in the KM-300-60 sample, the Kaol presence is still noticeable according to the peak at 440 °C on the DTG, making dehydroxylation still difficult at low temperatures. The broad DTG peak of KM-300-60 observed below 400 °C is attributed to the OH groups associated with the amorphised portion of the structure.

#### 3.2. Structural characterisation

Fig. 2 illustrates the crystallographic evolution of Kaol through XRD, as influenced by the different activation methods. This study primarily examines the degree of transformation of kaolinitic clay into an amorphous structure in the 5–40  $^{\circ}$ (2 $\theta$ ) diffractogram region. Most reflections in Fig. 2a are attributed to Kaol and quartz (Q) for K and KT-500. A

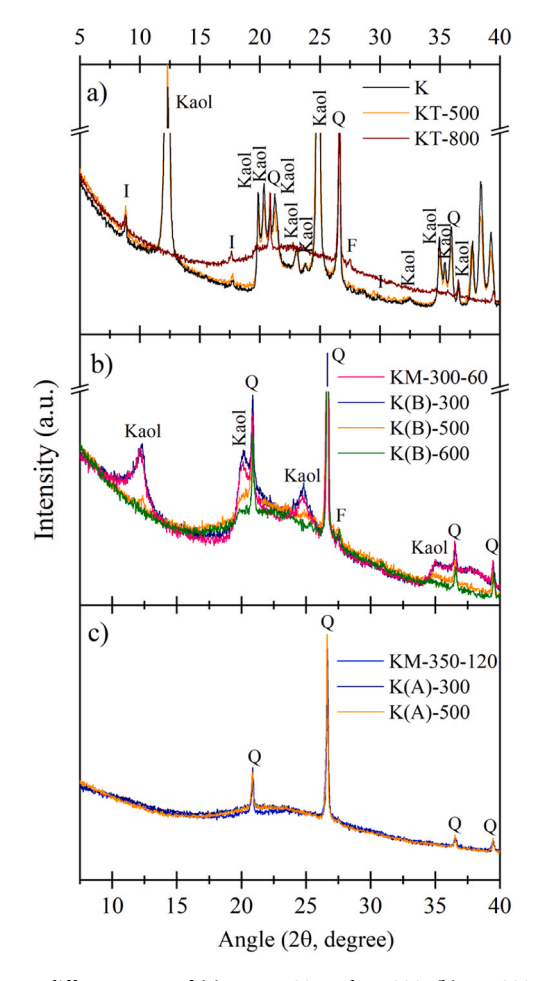


**Fig. 2.** XRD diffractograms of (a) K, KT-500, and KT-800, (b) KM-300–60 with its corresponding posterior thermal treatments, and (c) KM-350–120 with its corresponding posterior thermal treatments. Notations stand for Kaol=Kaolinite, I=Illite, Q=quartz, and F=K-feldspar.

comparison between them suggests a slight decrease in the kaolinitic reflections since a few OHs amount are released at 500 °C (see Fig. 1). Additionally, minor reflections at 8.8 °, 17.7 °, and 29.9 °(20) suggest the presence of secondary phases, likely illite and muscovite, and K-feldspar peaks appearing at 27.5 °(20).

The XRD pattern of the KM-300–60 sample displays reflections corresponding to Kaol and Q, suggesting that grinding at 300 rpm for 60 min only partially amorphises the structure (Fig. 2b). This is consistent with the presence of crystalline Kaol in its corresponding TGA (440  $^{\circ}$ C peak on DTG). Subsequent thermal treatments of the mechanically pre-treated samples are conducted to further reduce kaolinite reflections, aiming to disrupt this crystalline phase. The formation of an amorphised aluminosilicate source is evidenced by a broad humped peak within the 20–30  $^{\circ}$ (20) range [37].

Thermal activation of KM-300–60 at 300 °C, K(B)-300, does not alter the kaolinite structure significantly, as the kaolinitic reflections from KM-300–60 remained. Specifically, KM-300–60 requires 500 °C to accomplish almost the total elimination of kaolinitic reflections, expressing a substantial reduction in crystalline Kaol content for K(B)-500. Nevertheless, some low-intense reflections can be seen at 12.4 °, 19.9 °, and 24.9 °(20). At 600 °C the dehydroxylation is completed, as represented by the K(B)-600 sample.

A more intensive grinding process (KM-350–120) results in a diffractogram without Kaol reflections, as seen in Fig. 2c. XRD patterns of K (A)-300, K(A)-500, and even higher posterior calcination temperatures for KM-350–120 activation devoid kaolinitic reflections too. Comparing the XRD diffractograms of K(A)-500 or K(B)-500 with those of KT-500 evidences the effectiveness of amorphising the Kaol structure to a major degree with MTA at low temperatures instead of TA or MA (depending on the milling intensity). Moreover, the prior application of MA to MTA facilitates the partial amorphisation of other phases, such as quartz or illite, which cannot be activated through TA, generating more pozzolanic activity contributions. Based on this structural characterisation, less intensive mechanical grinding requires higher temperatures to achieve the total conversion of Kaol into an amorphous phase.

Foreseeing the thermal behaviour through thermogravimetric curves provides valuable insight into the effectiveness of MTA employment (Fig. 3). DTG data is also added (Fig. 3d, e, f) to plot the dehydroxylation rate thanks to MTA implementation. Moreover, Table 3 provides the mass loss attributed to all samples and the dehydroxylation degree achieved during the TA or MTA, expressed as the percentage of hydroxyls removed during calcination. This quantified data provides a deeper understanding of the MTA effect, based on the calculation procedure outlined in 2.4 (Eq. 2).

Figs. 3a and 3b demonstrate that the dehydroxylation can be efficiently trailed to low temperatures compared to the K dehydroxylation temperature (Fig. 3c) by implementing MTA. K thermal activation at 300 °C, 400 °C, and 500 °C has a minimal influence on the dehydroxylation degree. A slight reduction in hydroxyl groups is observable only at 500 °C, while calcination at 300 °C and 400 °C does not provide sufficient thermal energy to induce OH removal. On the contrary, mechanothermal activation allows a significant release of OHs at 300 °C, 400 °C, and 500 °C (Figs. 3a and 3b), evidencing the MTA effect in the reduction of the dehydroxylation temperatures required for Kaol. Notably, MTAs at 300 °C or 400 °C represents an interesting approach to the effectiveness of this process by enabling significant OH release that would not be attainable through calcination alone. For comparison, KT-300 and KT-400 exhibit OH release of only 0 % and 3.2 %, respectively, whereas the MTA unlocks a higher dehydroxylation degree, allowing a release of the OHs between 50 % and 72 %. In addition, MTAs at 500  $^{\circ}$ C produce almost complete dehydroxylation, while calcining untreated K at 500 °C appears to have minimal effect. The dehydroxylation levels achieved for K(A)-500 (85.7 %) and K(B)-800 (83.66 %) significantly exceed the effect observed in KT-500, which only releases 12.3 % of the OHs. However, implementing MTA at 600 °C provides a comparable dehydroxylation rate to conventional thermal activation at 600 °C since

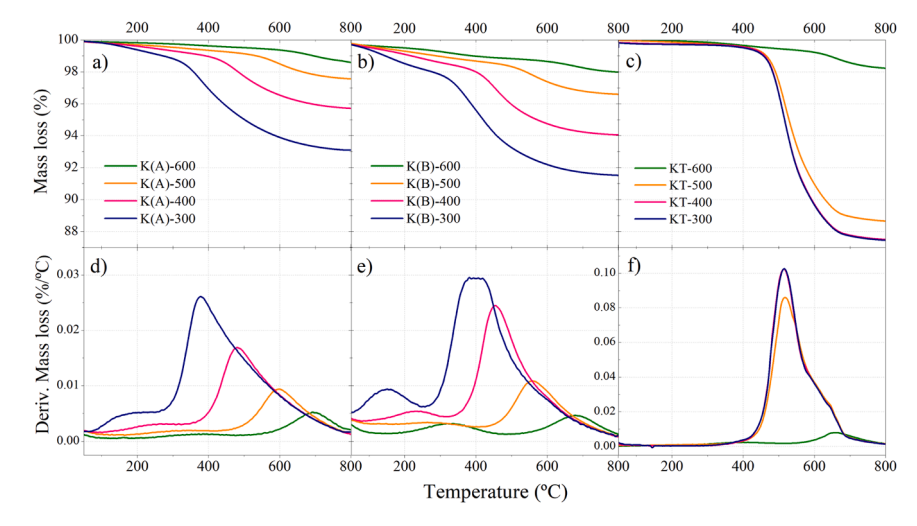


Fig. 3. TGA (a, b, and c) and DTG (d, e, and f) of mechanothermally treated samples (a, b, d, and e) and thermally treated samples (c and f).

Table 3
Dehydroxylation degree calculated through the TGA mass loss data.

	Mass loss from TGA (wt%)	Dehydroxylation degree (%)
K	12.71	-
KT-800	0	100
K(A)-600	0.69	93.7
K(A)-500	1.68	85.7
K(A)-400	3.41	71.9
K(A)-300	5.81	52.6
K(B) - 600	0.86	92.8
K(B) - 500	2.01	83.6
K(B)-400	4.4	65.1
K(B) - 300	6.57	46.9
KT-600	1.3	89.8
KT-500	11.15	12.3
KT-400	12.30	3.2
KT-300	12.71	0

the untreated K dehydroxylation predominantly takes place around 550–600 °C. This is supported by the values in Table 3: K(A)-600 achieves 93.7 % OHs release, K(B)-600 achieves 92.8 %, whereas KT-600 reaches a slightly lower but comparable value of 89.8 % OHs release. For this reason, the application of MTA at 600 °C becomes less effective in terms of the dehydroxylation rate, as well as for treatments at 800 °C.

On the other hand, using a more or less intensive grinding does not significantly change the enhancement of the dehydroxylation reduction (see the differences in Table 3), despite the structural variations observed in the XRD patterns. This indicates that complete structural disruption of kaolinite is not required for effective dehydroxylation when calcined at 500  $^{\circ}\text{C}$ .

Particle size distribution (PSD) and specific surface area evaluation are illustrated in Fig. 4 to track the morphological modifications induced by MA and MTA. The PSD of KM-350–120, K(A)-500, and K(A)-800 (Fig. 4a) exhibit a higher volume of particles within the 1–3  $\mu m$  range compared to K. Extending milling times or increasing rotation speeds in MA likely cause particle agglomeration due to formation of new chemical bonds through prolonged frictional interactions [27]. Furthermore, the particle diameters of the mechanothermally treated samples are even more concentrated within the 1–3  $\mu m$  range compared to KM-350–120, possibly due to sintering effects between particles induced by the heat exposure. This is evidenced by the decrease in the differential volume within the 6–10  $\mu m$  range. Consequently, K(A)-800 displays larger particles compared to K(A)-500, indicating increased sintering associated with higher thermal activation temperature.

Reducing milling impacts through less-intensive MA results in an

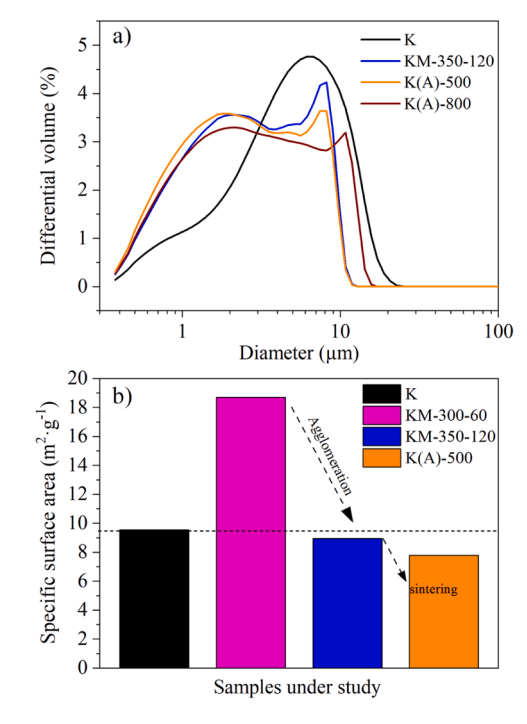


**Fig. 4.** Analyses of particle size distribution (a) and specific surface area (b) for representative samples activated through mechanical and mechanothermal methods, as well as K.

increase in specific surface area, as shown in Fig. 4b for KM-300–60. Additionally, the agglomeration effect at higher MA intensities is further supported by BET analysis represented by KM-350–120. Furthermore, the thermal application over a mechanically activated sample leads to a slight decrease in the specific surface area, likely attributed to a sintering phenomenon.

#### 3.3. Reactivity assessment

The reactivity measurements of the samples under study provided by the  $\rm R^3$  test are compiled in Fig. 5. Fig. 5a depicts the  $\rm R^3$  results of KM-300–60 and its derived samples activated through MTA, while Fig. 5b displays the corresponding data for KM-350–120. For comparative analysis, the thermally activated samples are represented in Fig. 5c. As expected, KM-350–120 (620.3 J·g $^{-1}$ ) can be classified as a more reactive

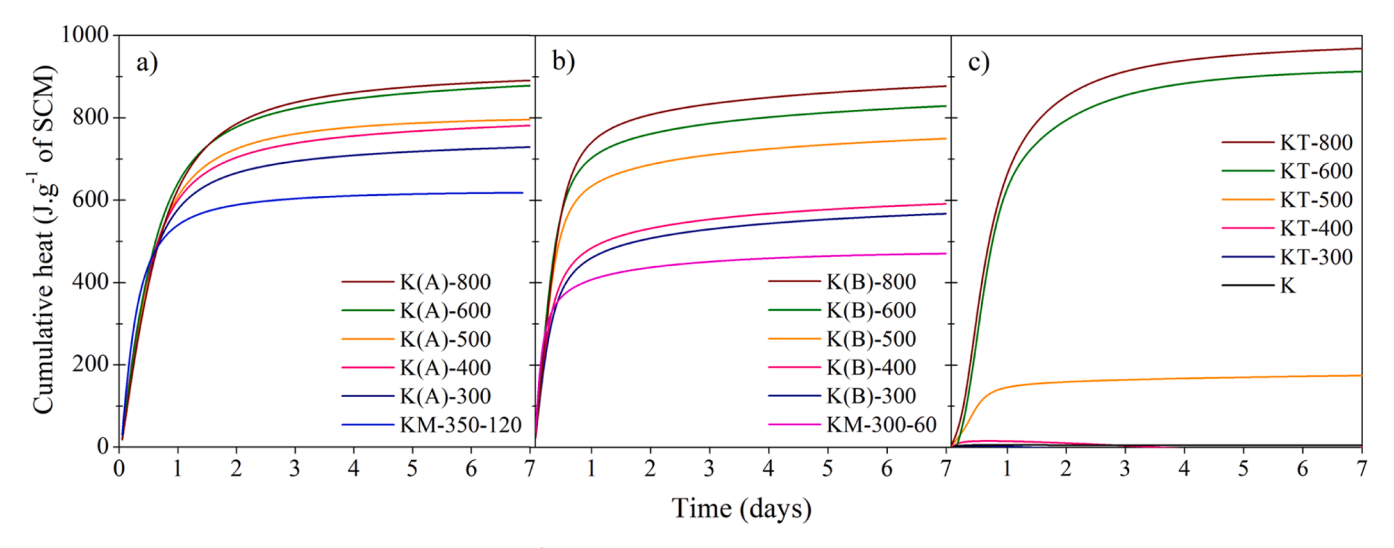


Fig. 5. R<sup>3</sup> test results of all MA, TA, and MTA samples.

material than KM-300–60 (470.5  $\rm J\cdot g^{-1}$ ), attributed to the difference observed in the amorphisation degree resulting from the initial MA.

MTA implementation demonstrates a highly efficient enhancement of reactivity values at low temperatures. Treating kaolin either thermally or mechanothermally results in significant differences in the pozzolanic activity of each activated samples. The most representative comparison occurs at 300 °C and 400 °C, where KT-300 and KT-400 present R<sup>3</sup> values of near zero at 7 days, likely due to the remaining unaltered kaolinitic structure after thermal induction at 300  $^{\circ}\text{C}$  and 400 °C. In contrast, K(A)-300, K(A)-400, K(B)-300 and K(B)-400 exhibit high pozzolanic activity due to the extended dehydroxylation achieved through MTA. Thus, MTA efficiently unlocks the dehydroxylation in K at 300  $^{\circ}\text{C}$  and 400  $^{\circ}\text{C}$ . Comparisons at 500  $^{\circ}\text{C}$  still remark the MTA effect. KT-500 increased from 174.2 J·g<sup>-1</sup> to very high pozzolanic numbers exceeding 700 J·g<sup>-1</sup> for K(A)-500 and K(B)-500, multiplying its effect on reactivity terms by a factor of 4. However, thermally activated K at 600 °C and 800 °C alone results in high pozzolanic values that mechanically activated samples cannot achieve.

The decrease in reactivity for all mechanothermally activated samples at 800  $^{\circ}$ C, related to metakaolin (KT-800), is quantified as a percentage in Fig. 6a-b (indicated by a red arrow). Since both methods appear to reach the same dehydroxylation rate, this reacting decrease may be explained through the sintering phenomenon of the particles observed in the PSD and BET study (Fig. 4). This reactivity reduction in

MTA at 800  $^{\circ}\text{C}$  compared to TA at 800  $^{\circ}\text{C}$  ranges from 8 % to 9.4 %, depending on the intensity of the initial mechanical application.

On the other hand, it is also remarkable that MTA provides superior reactivity values than MA across all samples. These increased pozzolanic values are also quantified in percentages in Fig. 6a-b (indicated by green arrows) to provide further information on MTAs' effects. Specifically, K (B)-500 highlights the efficacy of MTA, showing an increase in reactivity of 37.3 % in comparison with its MA, along with a substantial improvement over TA at 500  $^{\circ}\text{C}.$ 

As depicted in Fig. 7, XRD analysis of the resultant pastes from the R<sup>3</sup> test reveals the consumption of CH at the same time that tracks the formation of new hydrated phases, providing valuable insight into the reactivity rate. Representative samples with distinct reactivity values were selected to evidence the formation and consumption of these phases. Furthermore, Table 4 summarises the phases semiquantification through Rietveld refinement to provide more accurate data on phase consumption and formation.

Increased consumption of CH and calcite, caused by the reactions with amorphous aluminosilicates, indicates the reactivity of the activated kaolins. CH consumption promotes the formation of C-(A)-S-H phases, while calcite and CH consumption indicate the development of carboaluminate phases, specifically AFm phases such as hemicarboaluminate (Hc) and monocarboaluminate (Mc). In this regard, KT-800 exhibits the highest CH consumption compared to K(B)-500 and

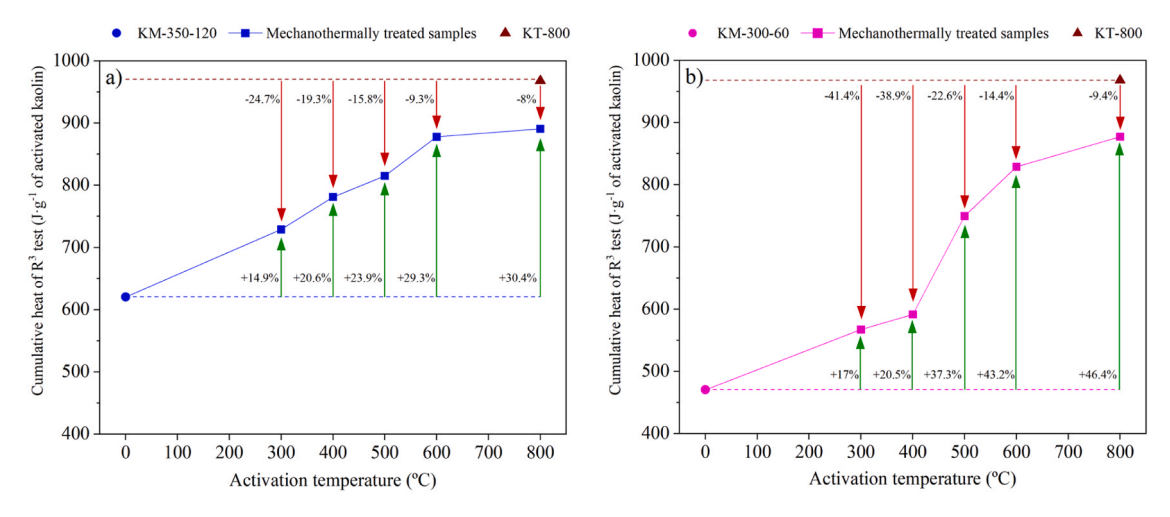
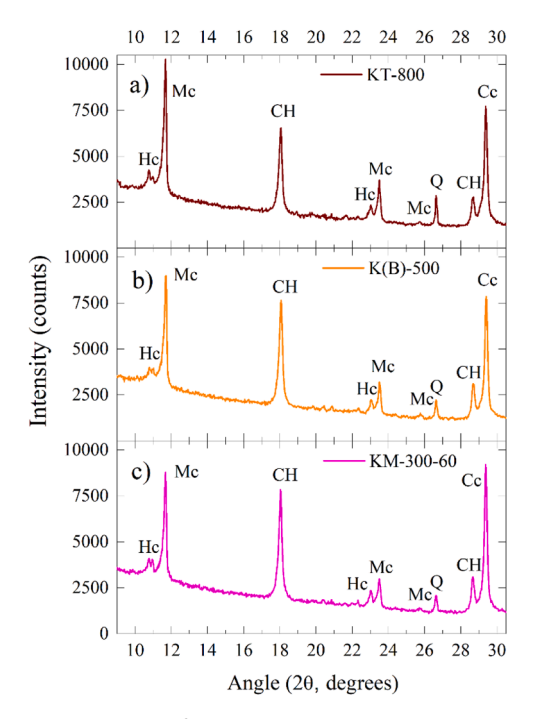


Fig. 6. Reactivity enhancement of MTAs compared to MAs (green arrow) and reactivity reduction of MTAs compared to KT-800 (red arrow) assessed through R<sup>3</sup> values at 7 days of mechanically activated samples, mechanothermally activated samples and KT-800.



**Fig. 7.** XRD pattern of the R<sup>3</sup> pastes from KT-800 (a), K(B)-500 (b), and KM-300–60 (c). The different phases are labelled as: CH=Portlandite, Cc=Calcite, Q=Quartz, Hc=Hemicarboaluminate, and Mc=Monocarboaluminate.

 $\begin{tabular}{ll} \textbf{Table 4} \\ \textbf{Percentage of crystalline and amorphous phases estimation of resultant $R^3$ pastes using Rietveld refinement.} \end{tabular}$ 

	Phases content (wt%)			
	KM-300-60	K(B)-500	KT-800	
Portlandite (CH)	30.00	30.74	24.49	
Calcite (Cc)	25.19	22.36	21.97	
Monocarbonate (Mc)	30.20	31.55	35.94	
Hemicarbonate (Hc)	5.63	5.36	6.27	
Amorphous	7.17	8.08	8.63	
Quartz (Q)	1.80	1.91	2.70	

KM-300–60, as evidenced by the significant reduction in reflections intensity, corroborated by Rietveld analysis results. Moreover, K(B)-500 presents a very slight decrease in CH content compared to KM-300–60. On the other hand, AFm phases are formed with KT-800 exhibiting the highest Hc and Mc content compared to K(B)-500 and KM-300–60. Furthermore, Mc formed in a major percentage for K(B)-500 than KM-300–60, whereas Hc presents a very similar formation rate. In particular, it can be observed that the Mc content is significantly higher than that of Hc across all R³ pastes from activated kaolins. In addition, the amorphous amount, mainly attributed to C-(A)-S-H hydrated phases, results in 7.17 % for KM-300–60, 8.08 % for K(B)-500 and 8.63 % for KT-800, corroborating the reactivity patterns with a linear trend where KT-800 > K(B)-500 > KM-300–60.

Fig. 8 illustrates the TGA and DTG data curves of pastes from the R<sup>3</sup> test, providing complementary evidence to the XRD patterns discussed earlier. Residual isopropanol can be observed at 82 °C as a consequence of the drying paste procedure. The formation of C-(A)-S-H and AFm is confirmed across all samples, as evidenced by the mass loss jump at around 100 °C and 130 °C, respectively [38,39]. The Mc and Hc formation is further corroborated by XRD results (Fig. 7), whereas the detection of C-(A)-S-H is more effectively performed using TGA, given the challenges in tracking its amorphous structure through XRD. The DTG curves reveal the decomposition of CH and calcite with distinct

peaks at approximately 400 °C and 650 °C, respectively.

In terms of reactivity behaviour, KT-800 exhibits higher consumption of CH and carbonates, resulting in the augmented formation of C-(A)-S-H and AFm phases compared to K(B)-500 and KM-300–60, as anticipated. However, K(B)-500 shows slightly higher CH consumption than KM-300–60, maintaining equal carbonate consumption. These findings reaffirm the reactivity trend as KT-800 > K(B)-500 > KM-300–60. Additionally, the DTG peaks observed at 265 °C and 340 °C could be attributed to amorphous AH<sub>3</sub> phases and C<sub>3</sub>ASH<sub>4</sub>, according to the literature [40]. Notably, the formation of the common phase in limestone calcined clay cement, ettringite (AFt), is not observed in either TGA or XRD, likely due to the absence of gypsum in R<sup>3</sup> pastes formulation [41].

Even though the R<sup>3</sup> test provides a more accurate simulation of cement reactions compared to the modified Chapelle test [37], it is implemented here to contrast the evidence of reactivity enhancement provided by the R<sup>3</sup> test data (see Fig. 9). Mechanically treated samples reached values according to their grinding intensity; KM-300-60 consumed 0.91 g of portlandite, whereas KM-350-120 fixed 1.28 g. These results indicate that MA alone is an effective activation method for kaolin with moderate pozzolanic activity. The posterior dehydroxvlation enhances portlandite consumption in mechanically activated K, showing a rising linear trend with increasing temperature for the MTAs. In addition, each subsequent thermal treatment of KM-350-120 surpasses the portlandite consumption of KT, even KT-600. Nonetheless, KT-800 performed as the highest pozzolanic material, with a 1.78 g consumed. The portlandite consumption measured for all the samples analysed in this investigation closely mirrors the R<sup>3</sup> values trend, where TA at 300  $^{\circ}$ C, 400  $^{\circ}$ C and 500  $^{\circ}$ C < MA < MTA < metakaolin (KT-800), corroborating the good correlation between both pozzolanic tests.

#### 3.4. Lab-scale energetic assessment

A preliminary lab-scale evaluation of the electrical consumption associated with different clay activation methods was conducted to furnish evidence about the MTA energetical impact (Table 5). However, this analysis offers only an initial estimate of the energy requirements, as current equipment used at the laboratory scale is not yet able to meet large-scale demand. Moreover, the lack of data referred to MA in industry applications implies some throwbacks to face the scalability challenges.

The left column from Table 5 evidences that the ball mills consume significantly less electrical energy than the furnaces, with the KT-T series exhibiting higher consumption compared to mechanically activated clays. For mechanothermally activated clays, energy consumption mainly depends on the thermal intensity applied during the MTA process. For temperatures below 500  $^{\circ}$ C, the process is less energy-intensive compared to metakaolin obtention (KT-800). In contrast, MTA processes at 600  $^{\circ}$ C or 800  $^{\circ}$ C require an even higher amount of energy, as they involve the combination of both mechanical and thermal activation processes.

Table 5 illustrates the energy consumption per gram of activated clay (Wh·g $^{-1}$ ) for each activation process. For both mechanical alone and mechanothermal activations below 600 °C, the energy required to activate 1 g of clay is lower compared to the KT-800 process (except for K(A)-600). Although this analysis is conducted at a laboratory scale using electrical data, the favourable performance of MTA suggests the potential for greater efficiency at the industrial level. Since the thermal activation of kaolin typically depends on fuel sources, scaling up could lead to a significant reduction in CO $_2$  emissions.

To estimate the efficiency of MTA in terms of reactivity yield relative to energy consumption, the energy use per unit weight is divided by the cumulative heat data from the R<sup>3</sup> test at 7 days. This calculation reveals the energy consumption required to achieve this level of reactivity per unit weight. For MTA treatments at 300 °C, 400 °C, and 500 °C, a significantly improved reactivity-to-energy ratio is observed compared

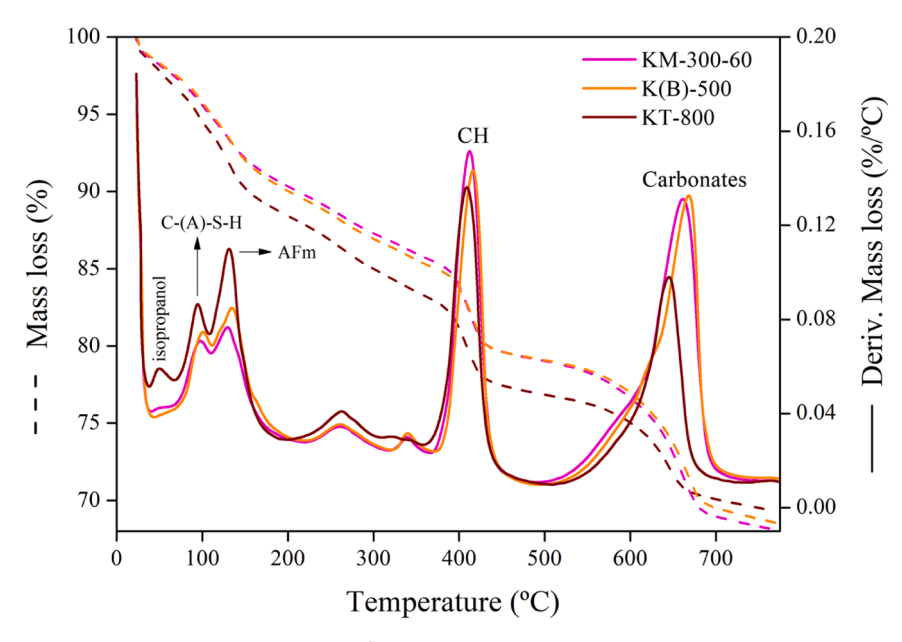


Fig. 8. TGA and DTG curves of the R<sup>3</sup> resultant pastes from KT-800, K(B)-500, and KM-300-60.

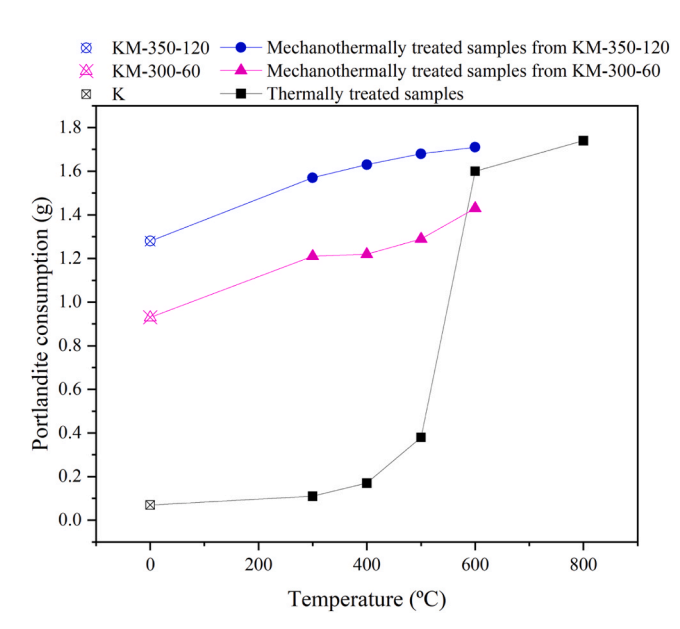


Fig. 9. Modified Chapelle test results of all MA, TA, and MTA samples.

to KT-300/400/500 samples. Nevertheless, despite increased reactivity, the energy demands of MTA are higher than those of mechanically activated kaolin.

#### 4. Conclusions

This study develops a multistep activation method for kaolinitic clays by combining mechanical activation (MA) with posterior calcination. This novel process reduces Kaol's dehydroxylation temperature related to the amorphisation of the structure induced by MA. Then, a thermal treatment is applied to release substantial amounts of OHs at much lower temperatures than conventional thermal activation (TA). Based on the structural changes monitored by characterisation techniques and pozzolanic tests, the following conclusions are summarised:

 As mechanothermal activation (MTA) conducts the posterior OHs release on the mechanically activated samples, the reactivity values

Table 5
Lab-scale energetic consumption of all MA, TA, and MTA samples.

	Energetic consumption of the activation method (Wh)	Energetic consumption normalised by the activated clay (Wh·g <sup>-1</sup> )	Electrical energy normalised by heat release from R <sup>3</sup> value (Wh·g <sup>-1</sup> ·J <sup>-1</sup> )
KM - 350 - 120	630	24.23	1.02
KM - 300 - 60	240	9.19	0.51
K(A)-800	2170	83.85	2.44
K(A)-600	1650	63.46	1.88
K(A)-500	1480	56.73	1.81
K(A)-400	1250	47.88	1.59
K(A)-300	1060	40.85	1.46
K(B)-800	1790	68.81	2.04
K(B)-600	1260	48.42	1.52
K(B)-500	1080	41.69	1.45
K(B)-400	850	32.84	1.44
K(B) - 300	670	25.81	0.92
KT-800	1550	59.62	1.60
KT-600	1020	39.23	1.12
KT-500	850	32.50	4.85
KT-400	620	23.65	133
KT-300	430	16.62	216

are higher if compared with MA, regardless of the grinding intensity, as demonstrated by the  $\rm R^3$  and modified Chapelle tests. In terms of reactivity, MTA outperforms MA (MTA > MA).

- TGA reveals a significantly higher dehydroxylation degree at 300 °C and 400 °C (approximately 50 % and 70 %, respectively), whereas thermally treated samples remain predominantly undehydroxylated. Consequently, reactivity increases substantially from near-zero values to high pozzolanic activity at these lower calcination temperatures. MTA unlocks the dehydroxylation at 300 °C and 400 °C.
- K(A)-500 and K(B)-500 achieve a significantly higher dehydroxylation degree compared to KT-500, with approximately 85 % and 12 %, respectively. In addition, K(A)-500 and K(B)-500 exhibited pozzolanic activity values only 15–20 % below that from metakaolin (KT-800), with a significant reduction in the calcination temperature of 300 °C. In contrast, KT-500 cannot be considered as a pozzolanic material since heat treatments at 500 °C have a minimal impact on the structure and reactivity. MTA demonstrates a strong capacity to highly dehydroxylate Kaol at 500 °C.

When applied at 600 °C or 800 °C, MTA produces less reactive materials than those achieved through TA alone, while also requiring more energy to be obtained. Consequently, MTA applied above 600 °C is considered inefficient.

This novel activation process effectively lowers the temperature required to produce metakaolin, reducing its environmental impact while aligning with the key findings. Unlocking the kaolinitic dehydroxylation at 300  $^{\circ}\text{C}$  and 400  $^{\circ}\text{C}$  ensures significant savings on fossil fuel sources. It highlights MTA as a promising approach for developing more sustainable activation methods. To maximise its potential, this strategy should be scaled up for industrial application to validate its effectiveness and feasibility in large-scale operations.

#### CRediT authorship contribution statement

Adrian Alvarez-Coscojuela: Writing – review & editing, Writing – original draft, Visualization, Methodology, Investigation, Formal analysis, Data curation, Conceptualization. Jofre Mañosa: Writing – review & editing, Supervision, Conceptualization. Josep Marco- Gibert: Investigation, Formal analysis. Javier C. Córdoba: Investigation, Formal analysis. Josep Maria Chimenos: Writing – review & editing, Visualization, Supervision, Funding acquisition, Conceptualization.

#### **Funding**

This work is partially supported by the Spanish Government with the Grant PID2021-125810OB-C21 funded by MICIU/AEI/10.13039/501100011033 and by ERDF/EU. The Catalan Government contributed with the Grant 2021 SGR 00708 through the Agència de Gestió d'Ajuts Universitaris i de Recerca (AGAUR).

#### **Declaration of Competing Interest**

The authors declare that they have no known competing financial interests or personal relationships that could have appeared to influence the work reported in this paper.

#### Acknowledgements

The authors would like to thank the Catalan Government for the quality accreditation given to their research group DIOPMA (2021 SGR 00708). DIOPMA is a certified agent TECNIO in the category of technology developers from the Government of Catalonia. The authors are grateful to the companies Minerals i Derivats, S.A. for the supply of the raw kaolin and the CCiTUB for the measurements of XRF, and XRD. The authors acknowledge the support of CYTED Network ECOEICo—Circular Economy as a Strategy for a More Sustainable Construction Industry and the COST Action CircularB—Implementation of Circular Economy in the Built Environment.

#### **Data Availability**

Data will be made available on request.

#### References

- [1] E. Gartner, Industrially interesting approaches to "low-CO2" cements, Cem. Concr. Res 34 (2004) 1489–1498, https://doi.org/10.1016/j.cemconres.2004.01.021.
- [2] L. Lavagna, R. Nisticò, An insight into the chemistry of cement—a review, Appl. Sci. 13 (2023), https://doi.org/10.3390/app13010203.
- [3] K.L. Scrivener, V.M. John, E.M. Gartner, Eco-efficient cements: potential economically viable solutions for a low-CO2 cement-based materials industry, Cem. Concr. Res 114 (2018) 2–26, https://doi.org/10.1016/j. cemconres.2018.03.015.
- [4] M.L. Nehdi, Clay in cement-based materials: critical overview of state-of-the-art, Constr. Build. Mater. 51 (2014) 372–382, https://doi.org/10.1016/j. conbuildmat.2013.10.059.

- [5] M.F. Brigatti, E. Galán, B.K.G. Theng, Structure and Mineralogy of Clay Minerals. in: Dev Clay Sci, Elsevier B.V, 2013, pp. 21–81, https://doi.org/10.1016/B978-0-08-08978-8-00002-Y
- [6] P. Suraneni, A. Hajibabaee, S. Ramanathan, Y. Wang, J. Weiss, New insights from reactivity testing of supplementary cementitious materials, Cem. Concr. Compos 103 (2019) 331–338, https://doi.org/10.1016/j.cemconcomp.2019.05.017.
- [7] P. Suraneni, J. Weiss, Examining the pozzolanicity of supplementary cementitious materials using isothermal calorimetry and thermogravimetric analysis, Cem. Concr. Compos 83 (2017) 273–278, https://doi.org/10.1016/j. cemconcomp.2017.07.009.
- [8] Y. Cao, Y. Wang, Z. Zhang, Y. Ma, H. Wang, Recent progress of utilization of activated kaolinitic clay in cementitious construction materials, Compos B Eng. 211 (2021), https://doi.org/10.1016/j.compositesb.2021.108636.
- [9] B.B. Sabir, S. Wild, J. Bai, Metakaolin and calcined clays as pozzolans for concrete: a review, n.d. (www.elsevier.com/locate/cemconcomp).
- [10] A.M. Rashad, Metakaolin as cementitious material: History, scours, production and composition-A comprehensive overview, Constr. Build. Mater. 41 (2013) 303–318, https://doi.org/10.1016/j.conbuildmat.2012.12.001.
- [11] A.A. Ramezanianpour, H. Bahrami Jovein, Influence of metakaolin as supplementary cementing material on strength and durability of concretes, Constr. Build. Mater. 30 (2012) 470–479, https://doi.org/10.1016/j. conbuildmat.2011.12.050.
- [12] R. Siddique, J. Klaus, Influence of metakaolin on the properties of mortar and concrete: a review, Appl. Clay Sci. 43 (2009) 392–400, https://doi.org/10.1016/j. clay 2008 11 007
- [13] V. Medri, E. Papa, J. Lizion, E. Landi, Metakaolin-based geopolymer beads: production methods and characterization, J. Clean. Prod. 244 (2020), https://doi. org/10.1016/j.jclepro.2019.118844.
- [14] F. Zunino, K. Scrivener, Reactivity of kaolinitic clays calcined in the 650 °C-1050 °C temperature range: towards a robust assessment of overcalcination, Cem. Concr. Compos 146 (2024), https://doi.org/10.1016/j.cemconcomp.2023.105380.
- [15] M. Georgiopoulou, G. Lyberatos, Life cycle assessment of the use of alternative fuels in cement kilns: a case study, J. Environ. Manag. 216 (2018) 224–234, https://doi.org/10.1016/j.jenvman.2017.07.017.
- [16] J. Mañosa, A.M. Gómez-Carrera, A. Svobodova-Sedlackova, A. Maldonado-Alameda, A. Fernández-Jiménez, J.M. Chimenos, Potential reactivity assessment of mechanically activated kaolin as alternative cement precursor, Appl. Clay Sci. 228 (2022), https://doi.org/10.1016/j.clay.2022.106648.
- [17] V.A. Baki, X. Ke, A. Heath, J. Calabria-Holley, C. Terzi, M. Sirin, The impact of mechanochemical activation on the physicochemical properties and pozzolanic reactivity of kaolinite, muscovite and montmorillonite, Cem. Concr. Res 162 (2022), https://doi.org/10.1016/j.cemconres.2022.106962.
- [18] J. Mañosa, J.C. de la Rosa, A. Silvello, A. Maldonado-Alameda, J.M. Chimenos, Kaolinite structural modifications induced by mechanical activation, Appl. Clay Sci. 238 (2023), https://doi.org/10.1016/j.clay.2023.106918.
- [19] A. Souri, H. Kazemi-Kamyab, R. Snellings, R. Naghizadeh, F. Golestani-Fard, K. Scrivener, Pozzolanic activity of mechanochemically and thermally activated kaolins in cement, Cem. Concr. Res 77 (2015) 47–59, https://doi.org/10.1016/j. cemconres.2015.04.017.
- [20] A. Mitrović, M. Zdujić, Preparation of pozzolanic addition by mechanical treatment of kaolin clay, Int J. Min. Process 132 (2014) 59–66, https://doi.org/10.1016/j. minpro.2014.09.004.
- [21] B. Ilić, V. Radonjanin, M. Malešev, M. Zdujić, A. Mitrović, Effects of mechanical and thermal activation on pozzolanic activity of kaolin containing mica, Appl. Clay Sci. 123 (2016) 173–181, https://doi.org/10.1016/j.clay.2016.01.029.
- [22] I. Balczár, T. Korim, A. Kovács, E. Makó, Mechanochemical and thermal activation of kaolin for manufacturing geopolymer mortars – comparative study, Ceram. Int 42 (2016) 15367–15375, https://doi.org/10.1016/j.ceramint.2016.06.182.
- [23] M. Fitos, E.G. Badogiannis, S.G. Tsivilis, M. Perraki, Pozzolanic activity of thermally and mechanically treated kaolins of hydrothermal origin, Appl. Clay Sci. (2015) 182–192, https://doi.org/10.1016/j.clay.2015.08.028, 116117.
   [24] J. Ondruška, Š. Csáki, V. Trnovcová, I. Štubňa, F. Lukáč, J. Pokorný, L. Vozár,
- [24] J. Ondruška, S. Csáki, V. Trnovcová, I. Stubňa, F. Lukáč, J. Pokorný, L. Vozár, P. Dobroň, Influence of mechanical activation on DC conductivity of kaolin, Appl. Clay Sci. 154 (2018) 36–42, https://doi.org/10.1016/j.clay.2017.12.038.
- [25] J. Mañosa, S. Huete-Hernández, A. Alvarez-Coscojuela, A. Maldonado-Alameda, J. M. Chimenos, Comparative study of limestone calcined clay cement produced with mechanically activated kaolin and calcined kaolin, J. Build. Eng. 97 (2024), https://doi.org/10.1016/j.jobe.2024.110748.
- [26] J. Mañosa, J.C. de la Rosa, A. Silvello, A. Maldonado-Alameda, J.M. Chimenos, Kaolinite structural modifications induced by mechanical activation, Appl. Clay Sci. 238 (2023), https://doi.org/10.1016/j.clay.2023.106918.
- [27] J. Mañosa, A. Alvarez-Coscojuela, A. Maldonado-Alameda, J.M. Chimenos, A lab-scale evaluation of parameters influencing the mechanical activation of kaolin using the design of experiments, Materials 17 (2024), https://doi.org/10.3390/ma17184651.
- [28] A.M. Rashad, Metakaolin as cementitious material: history, scours, production and composition-A comprehensive overview, Constr. Build. Mater. 41 (2013) 303–318, https://doi.org/10.1016/j.conbuildmat.2012.12.001.
- [29] F. Zunino, K. Scrivener, Reactivity of kaolinitic clays calcined in the 650 °C-1050 °C temperature range: towards a robust assessment of overcalcination, Cem. Concr. Compos 146 (2024), https://doi.org/10.1016/j.cemconcomp.2023.105380.
- [30] S. Hollanders, R. Adriaens, J. Skibsted, Ö. Cizer, J. Elsen, Pozzolanic reactivity of pure calcined clays, Appl. Clay Sci. 132-133 (2016) 552-560, https://doi.org/ 10.1016/j.clay.2016.08.003
- [31] A. Alvarez-Coscojuela, J. Marco-Gibert, J. Mañosa, J. Formosa, J.M. Chimenos, Thermal activation of kaolinite through potassium acetate intercalation: A

- structural and reactivity study, Appl. Clay Sci. 259 (2024), https://doi.org/
- [32] F. Avet, R. Snellings, A. Alujas Diaz, M. Ben Haha, K. Scrivener, Development of a new rapid, relevant and reliable (R3) test method to evaluate the pozzolanic reactivity of calcined kaolinitic clays, Cem. Concr. Res 85 (2016) 1–11, https://doi. org/10.1016/j.cemconres.2016.02.015.
- [33] Standard Test Methods for Measuring the Reactivity of Supplementary Cementitious Materials by Isothermal Calorimetry and Bound Water Measurements, (2020). https://doi.org/10.1520/C1897-20.
- [34] K. Weise, N. Ukrainczyk, E. Koenders, A mass balance approach for thermogravimetric analysis in pozzolanic reactivity r3 test and effect of drying methods, Materials 14 (2021), https://doi.org/10.3390/ma14195859.
- [35] X. Li, R. Snellings, M. Antoni, N.M. Alderete, M. Ben Haha, S. Bishnoi, Ö. Cizer, M. Cyr, K. De Weerdt, Y. Dhandapani, J. Duchesne, J. Haufe, D. Hooton, M. Juenger, S. Kamali-Bernard, S. Kramar, M. Marroccoli, A.M. Joseph, A. Parashar, C. Patapy, J.L. Provis, S. Sabio, M. Santhanam, L. Steger, T. Sui, A. Telesca, A. Vollpracht, F. Vargas, B. Walkley, F. Winnefeld, G. Ye, M. Zajac, S. Zhang, K.L. Scrivener, Reactivity tests for supplementary cementitious materials: RILEM TC 267-TRM phase 1, Mater. Struct. /Mater. Et. Constr. 51 (2018), https://doi.org/10.1617/s11527-018-1269-x.
- [36] E. Ferraz, S. Andrejkovičová, W. Hajjaji, A.L. Velosa, A.S. Silva, F. Rocha, Pozzolanic activity of metakaolins by the french standard of the modified chapelle test: a direct methodology, Acta Geodyn. Et. Geomater. 12 (2015) 289–298, https://doi.org/10.13168/AGG.2015.0026.
- [37] A. Alvarez-Coscojuela, J. Mañosa, J. Formosa, J.M. Chimenos, Structural characterisation and reactivity measurement of chemically activated kaolinite, J. Build. Eng. 87 (2024), https://doi.org/10.1016/j.jobe.2024.109051.
- [38] J. Yoon, K. Jafari, R. Tokpatayeva, S. Peethamparan, J. Olek, F. Rajabipour, Characterization and quantification of the pozzolanic reactivity of natural and nonconventional pozzolans, Cem. Concr. Compos 133 (2022), https://doi.org/ 10.1016/j.cemconcomp.2022.104708.
- [39] A.V. Soin, L.J.J. Catalan, S.D. Kinrade, A combined QXRD/TG method to quantify the phase composition of hydrated Portland cements, Cem. Concr. Res 48 (2013) 17–24, https://doi.org/10.1016/j.cemconres.2013.02.007.
- [40] E. Qoku, T.A. Bier, T. Westphal, Phase assemblage in ettringite-forming cement pastes: a X-ray diffraction and thermal analysis characterization, J. Build. Eng. 12 (2017) 37–50, https://doi.org/10.1016/j.jobe.2017.05.005.
- [41] Y. Zhang, J. Chang, J. Ji, AH3 phase in the hydration product system of AFt-AFm-AH3 in calcium sulfoaluminate cements: a microstructural study, Constr. Build. Mater. 167 (2018) 587–596, https://doi.org/10.1016/j.conbuildmat.2018.02.052.